Spatial quantification of leafless canopy structure in a boreal birch forest

T.D. Reid[a], M. Spencera, B. Huntley[b], S. Hancock[b, c], R.L.H. Essery[a], J. Carle[d], R. Holden[b], R. Baxter[b], N. Rutter[e]

[a] School of Geosciences, The University of Edinburgh, King's Buildings, West Mains Road, Edinburgh EH9 3JN, Scotland, UK

[b] School of Biological and Biomedical Sciences, Durham University, Durham DH1 3LE, England, UK

[c] School of Civil Engineering and Geosciences, Newcastle University, Newcastle upon Tyne NE1 7RU, England, UK

[d] Geospatial Research Ltd., Department of Earth Sciences, Durham University, Durham DH1 3LE, England, UK

[e] Department of Geography and Environment, Northumbria University, Ellison Building, Newcastle upon Tyne NE1 8ST, UK.

Highlights

•Leafless winter birch canopy affects snow energy balance in Arctic Sweden.

•Low-resolution (<1 m) airborne lidar used to obtain canopy heights on 4 m grid.

•Terrestrial laser scanning used to calibrate airborne lidar canopy heights.

•Canopy height and basal area strongly correlated to photo-derived sky view fraction.

•Sky view fraction estimated for 15 km^2 area using airborne data.

Abstract

Leafless deciduous canopies in boreal regions affect the energy available for snowmelt and reduce overall surface albedo during winter, thereby exerting a strong influence on weather and climate. In this work, ground-based measurements of leafless canopy structure, including hemispherical photography, terrestrial laser scanning (TLS) and manual tree surveys were collected at 38 sites in an area of mountain birch forest in northern Sweden in March 2011 and 2012. Photo-derived sky view fraction was strongly inversely correlated ($r < -0.9$) to the total tree basal area in a 5 m radius around the photo site. To expand findings to wider areas, maps of canopy height for a 5 km $\times$ 3 km area were obtained from airborne lidar (ALS) data collected during summer 2005. Canopy heights derived from TLS were used to validate the ALS estimates, and simple models were developed to establish relationships between hemispherical sky view and ALS canopy height (RMSE < 5%). The models and ALS data provide useful methods for estimating canopy radiative transfer and biomass over wide areas of birch forest, despite the relatively low ALS resolution ($\sim$1 return m^{-2}).

Keywords

- Boreal forests;
- Snow;
- Canopy radiative transfer;
- Airborne lidar;
- Terrestrial laser scanning;

- Hemispherical photography

Introduction

Arctic snow cover plays an important role in the climate system, due to the high albedo of snow-covered surfaces that reflect solar radiation back to space. The Arctic also contains large areas of forest that act to reduce overall surface albedo, even if snow is held in the canopy (Kuusinen et al., 2012). Under global warming scenarios, the combined effects of earlier snowmelt and expanding boreal forest cover could provide a positive feedback on warming; this is often termed the 'snow-albedo feedback' and has been shown to amplify warming for high northern latitudes in climate model experiments (Brovkin et al., 2009).

However, the interactions between snow and vegetation are very complex, and provide challenges for models of snow melt (Rutter et al., 2009). Trees intercept falling snow that can subsequently sublimate from the canopy top, and decrease the solar shortwave radiation reaching snow, while enhancing the thermal longwave radiation to snow from their warmed trunks and branches (Essery et al., 2007, Essery et al., 2008, Hardy et al., 2004, Link et al., 2004, Lawler and Link, 2011, Mahat and Tarboton, 2012 and Pomeroy et al., 2009). Conversely, snow cover could play an important role in future forest expansion; analysis of satellite products shows that snowy backgrounds enhance the absorption of photosynthetically active radiation near forest gaps, by reflecting radiation back up to the canopy (Pinty et al., 2011).

It is therefore important to improve quantification of the combined effects that snow and vegetation have on surface radiation and energy balance, on both local and regional scales. Such work requires detail on forest structure and canopy transmission. Hemispherical photographs ('hemiphotos') taken from the snow surface have been shown to provide excellent detail that can be used to estimate bulk canopy parameters such as leaf area index, or to track sun position for accurate calculations of the direct solar beam radiation component (Musselman et al., 2012a and Musselman et al., 2012b). Reid et al. (2013) combined this approach with sub-canopy radiation measurements to compare models of radiative transfer for boreal birch and conifer forests.

Considerably more detail can be obtained using high-resolution terrestrial laser scanners (TLS), which emit laser pulses and receive reflections from surrounding objects thousands of times per second, across a wide spherical field of view from the scanner position. Merging data from multiple scans of a canopy can produce a three dimensional cloud of points on the surfaces of canopy elements, in Cartesian co-ordinates with mm or sub-mm positional accuracy. Although TLS is expensive and time-consuming, it can be used to completely reconstruct trees in a virtual environment (Cote et al., 2009). Other recent efforts include using TLS to produce artificial hemiphotos that compare favourably to real hemiphotos (Seidel et al., 2012) and avoid some issues associated with optical camera methods such as lens vignetting or an insufficient contrast between canopy elements and the sky.

For the wider spatial characterisation of forests, airborne laser scanning (ALS), or lidar, has become widely used. For boreal forests, recent studies with ALS have aimed to quantify biomass (Kankare et al., 2013,Næsset et al., 2013 and Nyström et al., 2012) or identify treelines (Rees, 2007 and Thieme et al., 2011). ALS with high resolution (several returns per m^2) can be used to extract detailed canopy structure information that compares favourably to hemiphotos and can be extrapolated across large areas for the simulation of processes such as radiative transfer or precipitation interception (Varhola et al., 2012 and Musselman et al., 2013). However, there are clear benefits in trying to retrieve

canopy properties from relatively low resolution (~1 return per m^2) ALS data, because boreal canopy datasets of similar resolution are becoming available on national scales in e.g. Finland (Vastaranta et al., 2013), Sweden (Bohlin et al., 2012), Switzerland (Swiss Federal Office of Topography, 2013) and the USA (Stoker et al., 2008).

This paper presents canopy structure data collected during the spring snowmelt season in a leafless boreal birch forest. Correlations between the data, which include hemiphotos, manual surveys, TLS and ALS, are examined in order to estimate bulk canopy sky view on a 4 m grid, over several square kilometres.

2. Study site

The area near Abisko in Sweden (68.26–68.39° N, 18.50–18.82° E) contains wide areas of patchy, heterogeneous deciduous forest, mainly of mountain birch (*Betula pubescens* ssp. *czerepanovii*) that remain leafless for over six months of the year. Abisko is one of the world's most widely-studied Arctic landscapes and has experienced warming of 2.5 ° C from 1913 to 2006, with mean annual temperatures often exceeding 0 ° C and impacts that include changes to the tree-line (Callaghan et al., 2010). The focus of this study is a heterogeneous area of mountain birch forest to the south of Abisko village (Reid et al., 2013).

3. Data acquisition

3.1. Airborne lidar

The ALS data used in this paper were collected between 08:50 and 10:10 on 17 July 2005 using an Optech ALTM3033 scanning lidar belonging to the University of Cambridge Unit for Landscape Modelling (ULM). The instrument was mounted onboard the NERC ARSF Dornier 228 aircraft, which performed nine passes over the region at an average flying height of 2325 m above sea level (m.a.s.l.). Pulses of near-infrared laser radiation were transmitted at 33 kHz, with side-to-side scanning at 22.5 Hz and a swath of 39.6° corresponding to approximately 1250 m sampling width. Data were returned as pairs of first and last pulse returns at an average density of 0.72 paired returns per m^2.

For this study, a 5 km × 3 km portion of the ALS data was selected from the gentle north-facing slopes to the south of Lake Torneträsk, covering the tree-line transition from relatively dense birch coverage to open tundra (Fig. 1), with elevations ranging from 457 to 809 m.a.s.l.

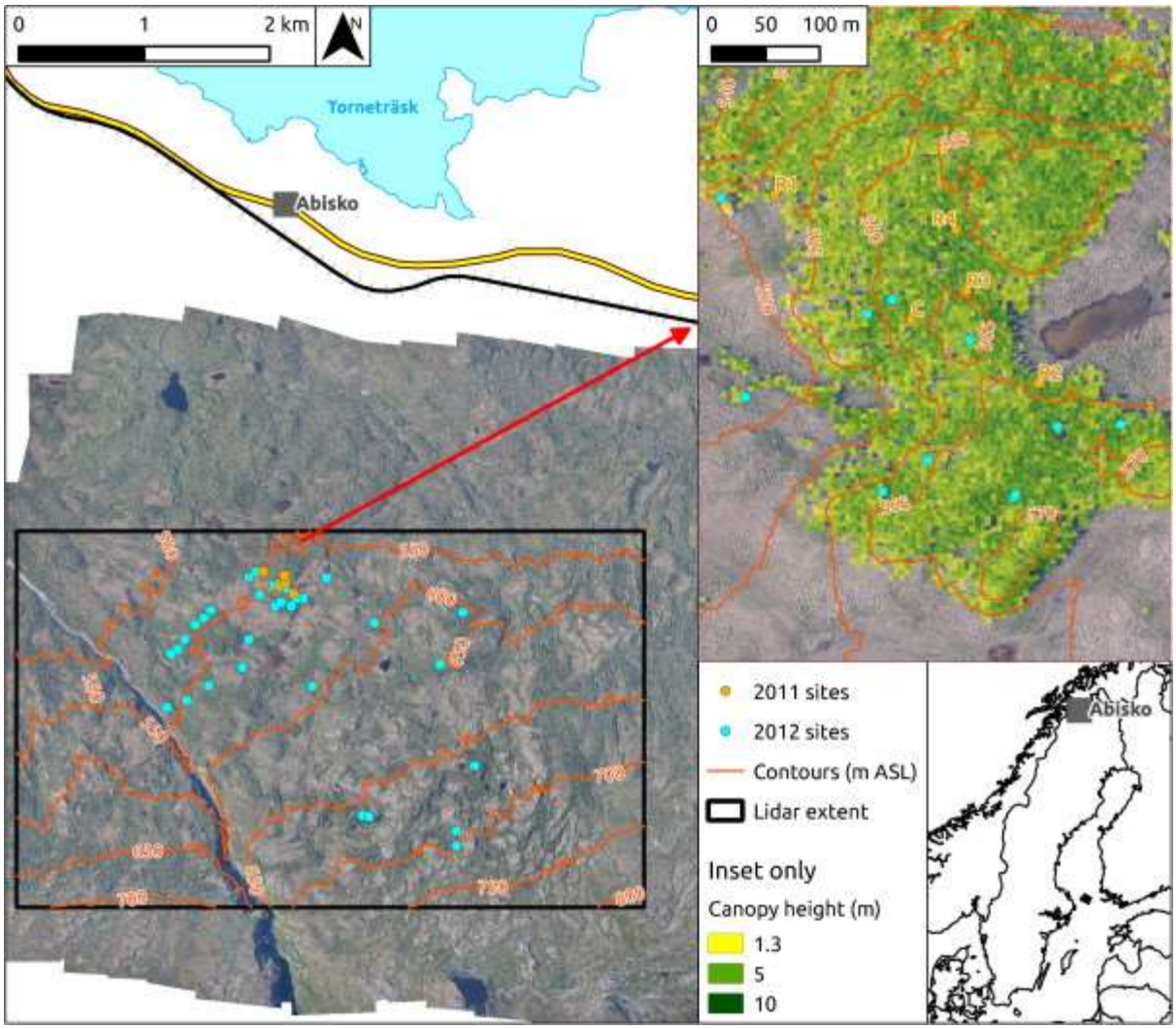

Fig. 1. Map of the Abisko study area with summer aerial photographs (see Acknowledgements) georeferenced onto the 5 km × 3 km ALS area selected for this study. The forest plots established in 2011 and the hemiphoto sites from 2012 are shown, and canopy heights are shown on the close-up. Scandinavian context map taken fromhttp://thematicmapping.org/downloads/world_borders.php; Abisko map details © OpenStreetMap contributors.

3.2. Hemispherical photography

Five 20 m × 20 m forest plots of various densities, named C, R1, R2, R3 and R4, were established in March 2011 (Reid et al., 2013) close to 68.32° N, 18.83° E, towards the centre north of the 5 km × 3 km ALS-sampled square (Fig. 1). To characterize the canopy, upward-looking hemiphotos were taken using a Nikon Coolpix 4300 digital camera with a Nikon FC-E8 fisheye converter lens, positioned on a small tripod approximately 30 cm above the top of the snowpack. Ten photographs were taken in each plot in the configurations shown in Fig. 2(a).

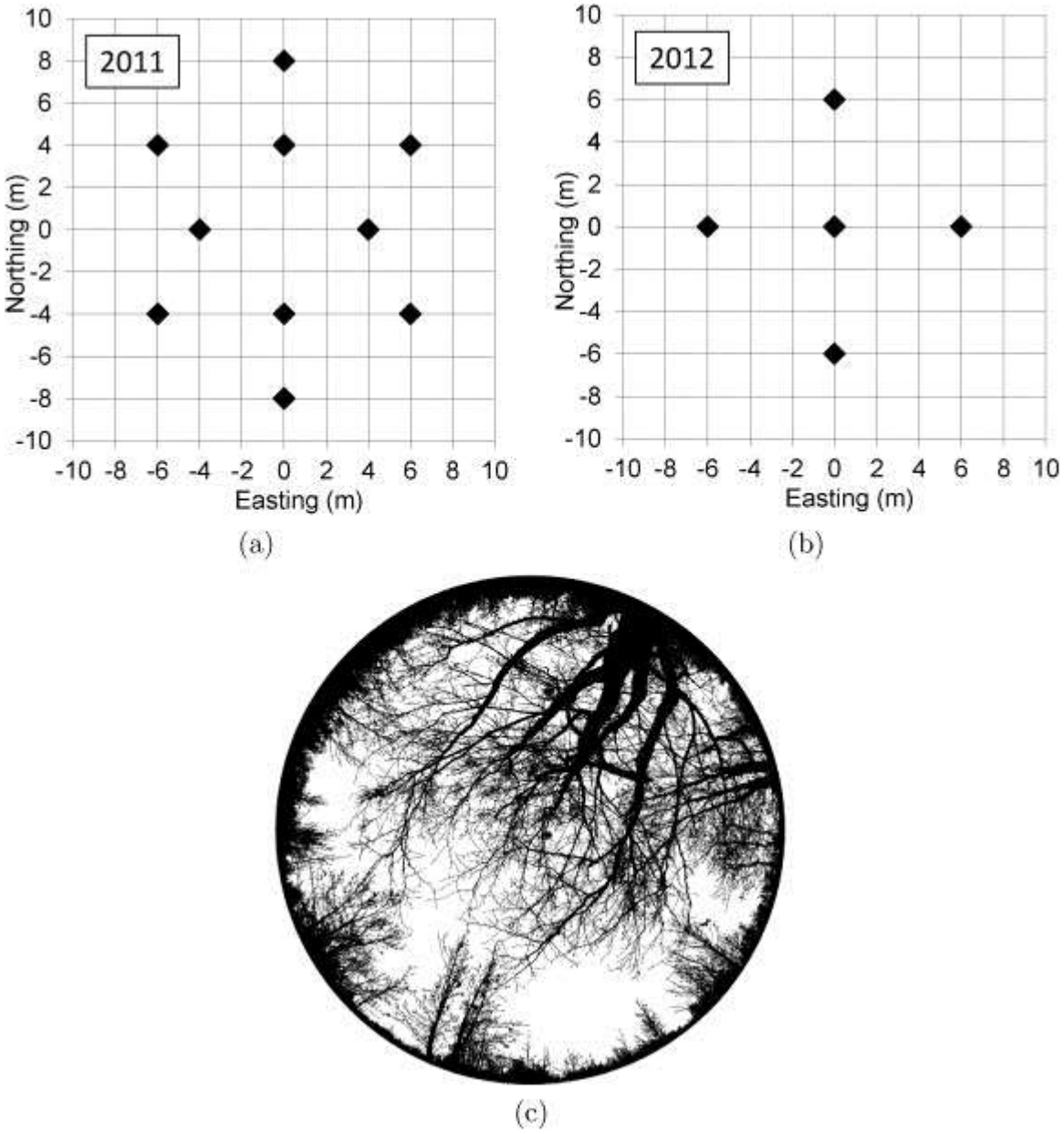

Fig. 2. Positions at which hemiphotos were taken for (a) the five 20 m × 20 m forest plots in 2011 and (b) the thirty-three wider-scale samples in 2012. Centre positions (0, 0) were measured using dGPS for comparison to the ALS and (c) an example of a processed binary hemiphoto from Abisko.

In March 2012, further hemiphotos were taken to sample the canopy in the wider area up to and including the treeline. Thirty-three sites were sampled by taking five photographs at each site, starting with a central point before sampling points 6 m away in all four cardinal directions (Fig. 2(b)).

Hemiphotos were processed via manual thresholding to produce binary representations separating canopy and sky. As demonstrated in Reid and Essery (2013) and Reid et al. (2013), automatic thresholding methods such as that of Nobis and Hunziker (2005) were not possible for hemiphotos

of the sparse, leafless Abisko canopies due to the lack of high-contrast edges between the light-coloured birch elements, snowy horizons and sky, and a lack of perfectly overcast conditions that were not accompanied by snowfall. Instead, careful manual thresholding, manual shading of the snowy horizon, and the branch joining algorithm described in Reid and Essery (2013) were applied using bespoke software. Fig. 2(c) shows an example. Values of gap fraction, v_θ, were calculated as the ratio of sky pixels to total pixels in concentric bands of elevation angle (ϑ) in the hemisphere. Values of hemisphere-averaged sky view fraction v_s were calculated from v_θ as in Essery et al. (2008).

3.3. Terrestrial laser scanning

During the March 2011 field campaign, a Leica ScanStation C10 terrestrial laser scanner (TLS) was used to provide detailed 3D representations of the birch canopy in the five forest plots. In each plot, the scanner was positioned on a tripod at scan positions chosen subjectively to sample the canopy as thoroughly as possible; between 5 and 7 scans were performed in each plot depending on the canopy density. Every scan was performed on the medium resolution setting, which provided 0.0573° sampling, corresponding to a beam spacing of 1 cm at 10 m distance from the scanner. Ten target spheres of known diameters (four 6-in. and six 4.5-in.) were placed in fixed positions on stakes in the snow for all the scans in a plot. Separate fine-resolution scans were made of as many target spheres as were practically visible from each scanner position; this required some manual bending of branches and shrubs out of the way. Leica Cyclone software (Leica, 2013) was used to stitch data from different scans together based on the target sphere positions, producing a single point cloud for each forest plot with sub-cm positional errors. To transform the scan coordinates to UTM, plot corner posts – which had been geo-located using a Trimble R8 differential global positioning system (dGPS) – were identified in the point cloud, and Powell's method (Press et al., 1992) was used to minimise the RMSE of a transform between the coordinate systems.

3.4. Manual tree measurements

To quantify the forest canopy further, a manual survey of the five 20 m × 20 m forest plots was undertaken between 30 June and 7 July 2011 (this work was easier to perform in snow-free summer conditions, and woody biomass does not change significantly between March and June). The number of trees was counted and, given the extremely polycormic character of many of the trees, the number of individual trunks arising from each rootstock, and thus forming one tree, was also recorded. It should be noted that some trunks just outside the plot boundaries were also measured because their canopies extended into the plots. The girth at breast height G (cm), at 1.3 m above the ground, of each individual trunk was measured using a dressmaker's tape; to qualify as a trunk a stem had to arise from the rootstock (i.e. it was not a branch of another trunk) and either reach a height ≥ 3 m or have $G \geq 5$ cm. The effective basal area (cm^2) of each trunk was calculated as $G^2/4\pi$; the basal area of the tree was then the sum of the basal areas of its trunks, and the total basal area for the plot was the sum of the basal areas of the trees. Each tree was labelled when measured so as to ensure no trees were missed or measured more than once, and the location of each was recorded using the

dGPS. The presence of the canopy as well as the complex topography necessitated accepting some degradation of the potential precision of the dGPS system in order to obtain positions for the trees; a horizontal precision of ±20 cm was nonetheless achieved in all cases, and for most trees the precision achieved was ±10 cm or better. The position recorded was as close to the trunk as possible in the case of single trunked trees, and as near to the centre of the rootstock as possible in the case of polycormic individuals.

4. Result and analysis

4.1. Airborne vs. terrestrial canopy height

The average density of ALS returns was 0.76 first-and-last-return pairs m^{-2}, and this value was fairly consistent at all the ground sample sites despite some minor spatial heterogeneity over the wider area caused by overlapping flight paths. The lidar system had a beam divergence setting of 0.5 mrad, which corresponds to ground spot radii of 38–47 cm for the range of flying heights above the ground. On comparing these spot radii to the return density, and considering the likelihood that the first returns did not always reflect from the highest canopy elements, the lidar clearly did not sample the entire canopy; some binning of returns into larger footprints is required to obtain the best estimates of canopy height. This approach is supported by pioneering lidar studies including Zimble et al. (2003), Drake et al. (2002) and Lefsky et al. (1999) who showed that lidar coverage needs to be large enough to ensure that some returns are received from the ground and some from tree tops, while remaining small enough to be sensitive to the contribution of individual crowns. Those authors used 5–30 m footprints for their study areas which included large temperate trees; at Abisko we argue that 4 m × 4 m pixels are suitable to allow for the sparsity of the canopy and discrete returns of the lidar points.

Returns were binned into the relevant 4 m squares, giving an average of 12.15 returns per pixel. Canopy height h_{ALS} for each pixel was calculated as the maximum of all first-return heights minus the minimum of all final-return (ground) heights in the square, as described in Hofton et al. (2000). As argued in Hancock et al. (2011), such low resolution ALS will almost certainly underestimate canopy height by missing the tallest parts of trees, and overestimate ground height due to understory; for these reasons a comparison to TLS ground data was performed. Under some conditions it could be argued that this approach may slightly underestimate ground height due to sloping of terrain within the pixel, but the effects of this should be minimal given the fact that the majority of ground sites were quite flat. Furthermore, Hancock et al. (2012) describe how understory elements, or any other low lying objects such as twisting tree trunks, can lead to overestimates of ground heights.

The TLS data (processed into x, y, z format representing UTM easting, northing, and m above sea level) were binned into 1 m × 1 m horizontal pixels, and the lowest return in each pixel was identified. Returns were then binned into 10 cm vertical bins of ‘height above lowest return’ for each pixel. Fig. 3 shows the average return profile for each forest plot. In all five plots, the ground returns show a spike at 30–40 cm, which is likely the snow surface; returns from lower heights are likely from paths

bashed through the snow by researchers. For this reason, canopy height above snow was defined for every square metre as the difference between the height of the highest return and the height of the bin containing the greatest number of returns (Hofton et al., 2000, Hofton et al., 2002 and Rosette et al., 2008). If this value was found to be less than 0.5 m it was assumed that these returns could be caused by variation in snow height, and the pixel canopy-above-snow height was set to zero, implying a vegetation-free pixel.

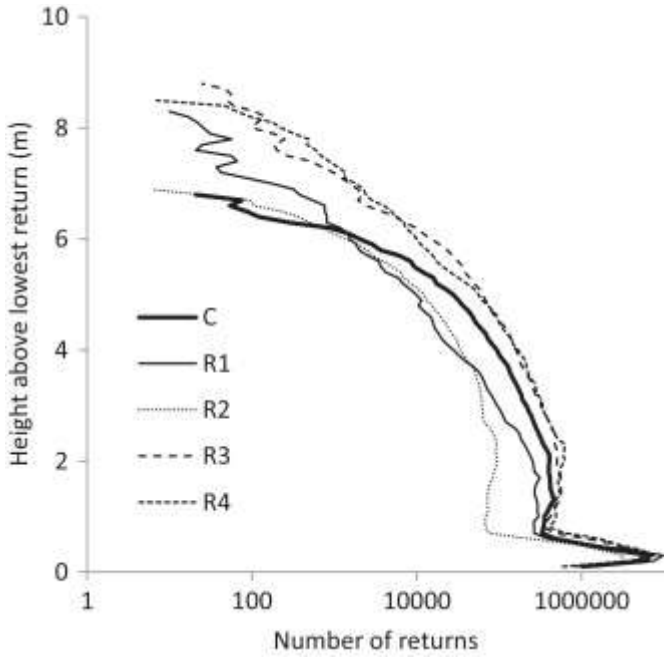

Fig. 3. Average TLS return profiles for the five 20 m × 20 m forest plots. For every square metre, returns were counted in bins of 10 cm intervals of height-above-lowest-return.

To correct the TLS canopy heights to height-above-ground rather than height-above-snow required snow depth measurements, which were made on a 2 m grid providing 121 measurements per plot. These measurements were not made on days of scanning, but at most 7 days before scanning in each plot; the average 7-day range (maximum minus minimum) across daily snow depths recorded by observers at Abisko Scientific Research Station over the study period was only 7.4 cm, suggesting that errors due to snowfall or compaction at the forest plots will be small. Given the positional errors in comparing snow depth measurements made using manual compass and measuring-tapes to geo-located TLS data, uncertainty in snow depth due to unseen underlying topography, and the unknown wind redistribution of snow over time, it was not deemed worthwhile applying individual snow depth corrections to every pixel. Instead the mean snow depths for each plot were added on to all non-zero TLS canopy heights. The mean and standard deviation of canopy height calculated in this way for each forest plot are shown in Table 1.

Table 1. Mean and standard deviation (σ) of canopy height obtained from the TLS point cloud, and the number of 1 m^2 squares used for calculating the mean (required to have at least 1000 laser returns).

Plot	Mean (m)	σ (m)	Squares used
C	3.52	1.91	1139
R1	1.78	1.87	976
R2	2.85	2.41	997
R3	4.80	1.84	1107
R4	3.86	2.33	1319
All	3.43	2.31	5538

To compare the summer ALS to the winter TLS canopy heights, any airborne canopy heights below 1.3 m were set to zero to match the processing performed on the TLS data (0.5 m variation threshold plus 0.80 m snow depth – the mean across all plots). For every 4 m airborne pixel, the following protocol was followed:

1 Find all 1 m^2 TLS pixels within the airborne pixel.

2 If there are fewer than ten such TLS pixels, ignore this airborne pixel.

3 Remove any poorly sampled TLS pixels, defined as those containing fewer than 1000 laser returns.

4 If there are still more than five TLS pixels left after step 3, select the mean TLS canopy height from these remaining TLS pixels.

This process of sampling the TLS led to paired airborne-TLS datapoints. Fig. 4(a) and Table 2 show that there was considerable scatter in the relationship between the airborne and TLS methods, including several points on the *x* or *y* axes where one of the methods gave a zero canopy height while the other showed canopy to be present. To investigate whether this was an artefact of spatial offsetting between the two methods, the ALS coordinates were adjusted in steps of 1 m from −10 to +10 m easting and northing. Fig. 5 shows the distribution of the correlation coefficient *r* on applying these offsets to the five forest plots individually, and all together. For every plot except R3, the optimum easting and northing offsets were similar, and are reflected in the optimum offsets of −5 m northing and −5 m easting when all plots were adjusted together giving a correlation of $r = 0.30$. R3 shows lower sensitivity to the spatial offsets, as might be expected given that it showed the lowest percentage standard deviation in canopy height (Table 1) and was observed to be subjectively the most dense plot sampled with the most consistent tall, thin trees. As shown in Fig. 4(b) and Table 2, applying the optimum offsets resulted in less scatter of the datapoints as well as fewer airborne 'misses' (points where the airborne canopy height was 0 m but TLS canopy height was non-zero) and no ground misses. It is impossible to correct for the airborne misses – which account for 9% of the sampled 4 m × 4 m pixels – in any areas other than the five 20 m × 20 m forest plots. The more general underestimation of canopy height by the airborne data relative to TLS is expected given the far lower number of airborne sampling points, which will generally miss the highest canopy elements.

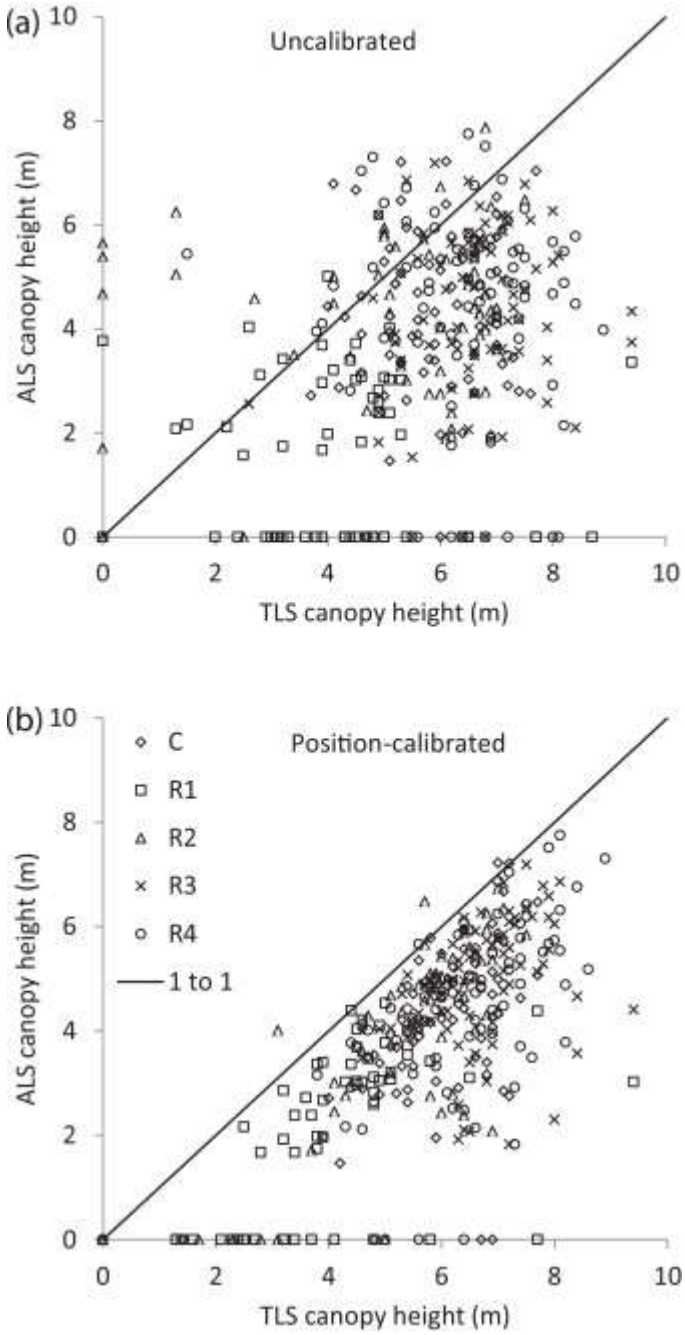

Fig. 4. Scatter of canopy heights obtained from ALS and TLS (a) using UTM coordinates without adjustment and (b) using calibrated coordinates based on the optimum offsets found in Fig. 5 (−5 m easting and −5 m northing applied to the airborne coordinates). Legend in (b) also applies to (a). Fit statistics are in Table 2.

Table 2. Statistics of correlations between ALS and TLS canopy heights for the uncalibrated and position-calibrated situations shown in Fig. 4, including correlation coefficient (*r*), root mean square error (RMSE), mean bias deviation (MBD) and the equation of a linear regression. 'Airborne misses' refers to points where the airborne canopy height was 0 m but TLS canopy height was non-zero (vice versa for 'ground misses').

	Uncalibrated	Calibrated
Number of points	344	345
r	0.29	0.73
RMSE	2.93 m	2.28 m
MBD	−1.92 m	−1.83 m
Regression	$h_{ALS} = 0.33h_{TLS} + 1.91$	$h_{ALS} = 0.78h_{TLS} - 0.57$
Airborne misses	42	31
Ground misses	5	0

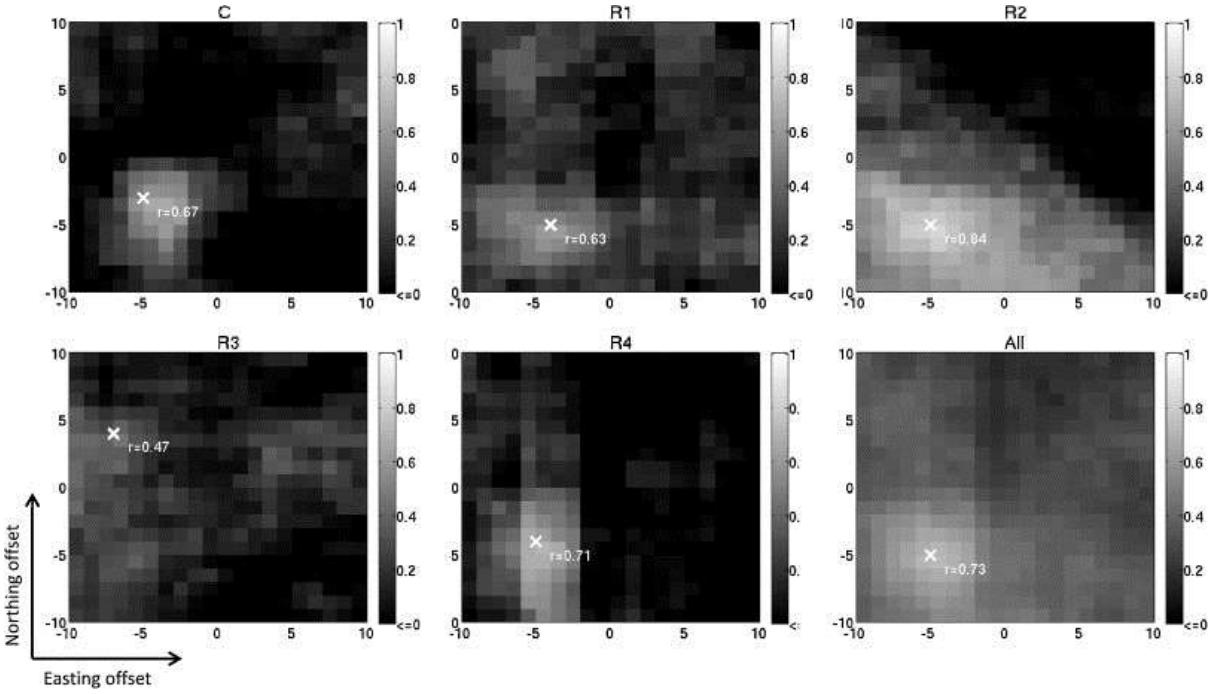

Fig. 5. Correlation coefficient (*r*) between ALS and TLS obtained upon offsetting airborne coordinates in 1 m intervals of easting and northing, for the five forest plots (C, R1–4) and for all plots combined (lower right). The positions of best correlation (highest *r*) are indicated by crosses.

For the remainder of this paper, the offsets of −5 m in both easting and northing are applied to the ALS coordinates, and the airborne canopy height data are adjusted to 'true' canopy height represented by the TLS by inverting the calibrated linear regression formula in Table 2.

4.2. Tree basal area vs. canopy height

The main results from the manual tree survey are shown in Table 3. The polycormic nature of most of the trees is apparent, especially in plot C which had on average 5.53 trunks per tree. Plot R3 had the greatest total basal area, although R4 had the greatest mean basal area per tree and thickest trunks on average. Fig. 6 shows the two datasets together and verifies that the trunks correspond well with the tallest areas of canopy. Table 4 shows that there were weak positive correlations between manual tree basal area and TLS canopy height in the trunk-containing pixels, for all five forest plots.

Table 3. Summary of manual survey data for each forest plot.

Plot	No. trees	No. trunks	Mean no. trunks per tree	Total BA (% ground)	Mean BA per tree (cm^2)	Mean BA per trunk (cm^2)
C	40	221	5.53	0.078	77.96	14.11
R1	28	67	2.39	0.030	43.11	18.01
R2	37	125	3.38	0.046	50.12	14.84
R3	113	326	2.88	0.149	52.66	18.25
R4	50	183	3.66	0.129	103.60	28.31
All	268	922	3.44	0.087	64.59	18.77

BA, basal area.

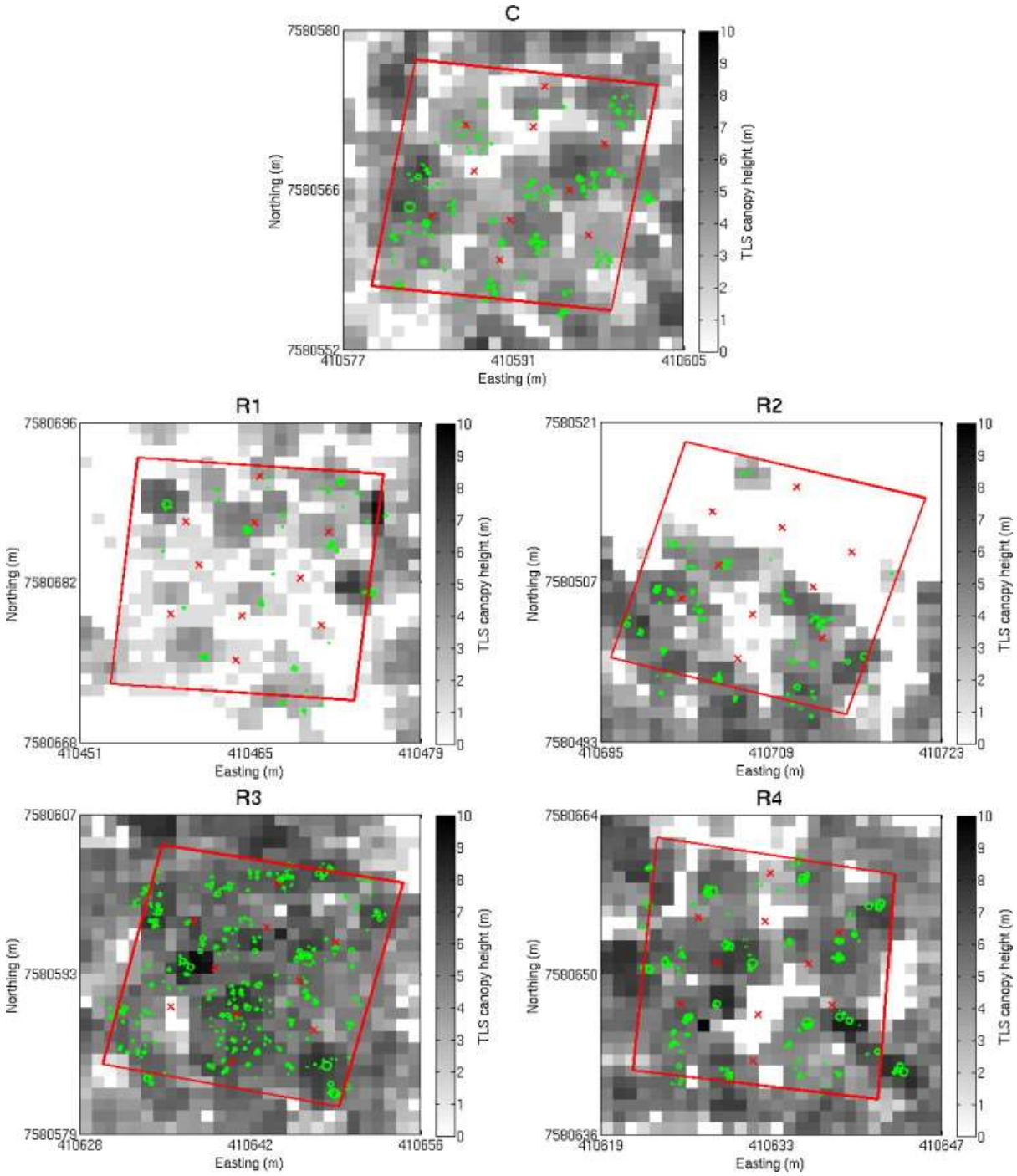

Fig. 6. Comparison of TLS canopy height and manual tree basal area measurements. Measured trunks are in green with radii scaled up by a factor of 5 for clarity. Plot boundaries and hemiphoto positions (*x*) are in red. Original plot boundaries were set out manually using compass and measuring tape; rotation and skewness are due to magnetic declination and topography. Note some trunks outside the plots were measured because their canopies extended into the plots. (For interpretation of the references to colour in this figure legend, the reader is referred to the web version of the article.)

Table 4. Correlation (*r*) between tree basal area and TLS canopy height for the forest plots. 'No. trunk pixels' means the number of 1 m^2 pixels containing trunks that were used to obtain the correlations.

Plot	No. trunk pixels	*r*
C	102	0.37
R1	35	0.58
R2	50	0.40
R3	167	0.29
R4	74	0.36
All	428	0.30

These data provide an opportunity for comparison to the findings of Dahlberg et al. (2004), who sampled 46 mountain birch trees in the Abisko area to obtain dry weights of leaves, stems and branches for individual trees; they obtained strong relationships between these weights and tree parameters such as total basal area at breast height, *TBA*, and tree height, *H*. For winter studies, the dry weight of wood, *DWW*, equivalent to stems plus branches, is most relevant. Dahlberg et al. (2004) obtained the following relationship between *DWW* and *TBA*:

equation(1)

$$\ln DWW = -1.1148 + 0.9994 \ln TBA$$

where *DWW* is in kg and *TBA* is in cm^2. On including *H* in the model, they obtained:

equation(2)

$$\ln DWW = -1.8766 + 0.6608 \ln TBA + 1.1935 \ln H$$

where *H* is in m. Combining Eqs. (1) and (2) produces the following relationship between *TBA* and *H*:

equation(3)

$$TBA 0.1054 H^{3.5248}$$

Fig 7(a) shows the model curve of Eq. (3) plotted with data for every pixel containing trunks in Fig. 6, with*TBA* expressed as the fraction of trunk coverage within each 1 m^2 pixel. There is considerable scatter, and many outliers where it is likely there were several trunks in each pixel, or the highest points of the trees were not directly above the stem location; indeed this pixel-based approach is strictly not directly comparable to the Dahlberg model which was based on measurements of individual trees. However, the orders of magnitude of the data and the model are similar, likely because there was usually no more than 1 tree per square metre. More detailed analysis of TLS data (Cote et al., 2009) would allow a better comparison to manual data and more accurate estimates of other biophysical parameters of trees.

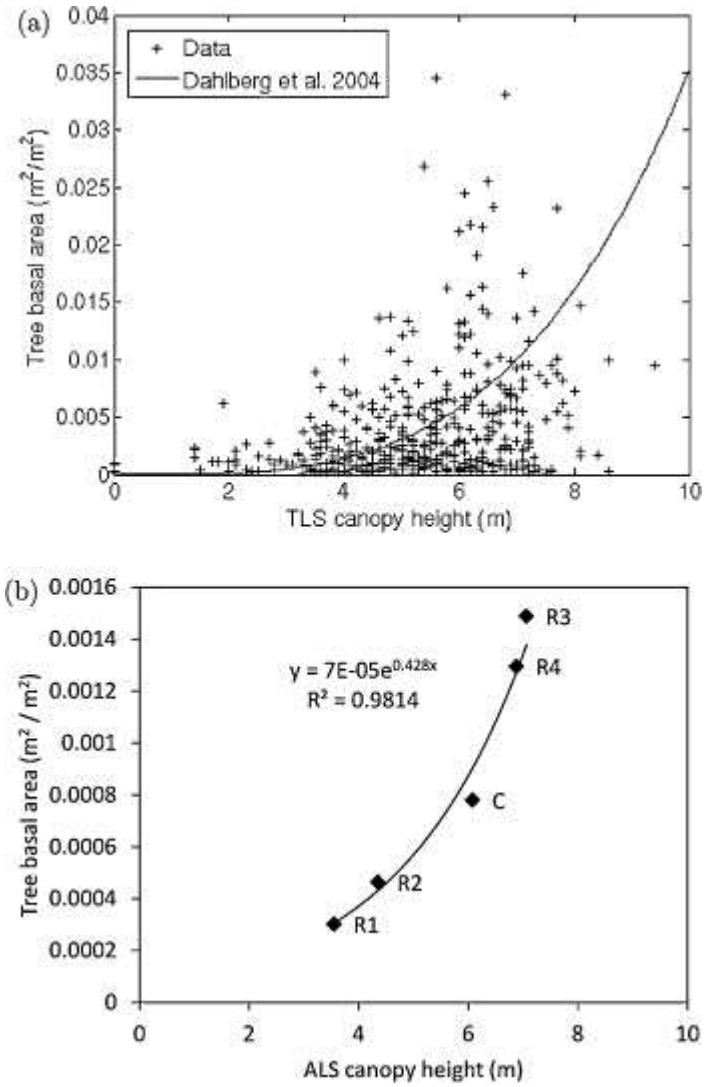

Fig. 7. (a) Scatter of tree basal area against TLS canopy height where each cross represents one of the 1 m^2 pixels containing trunks in Fig. 6; a model derived from the work of Dahlberg et al. (2004) is superimposed and (b) average basal area fraction against average ALS canopy height for whole forest plots.

For wider-scale classification of forest density, it is useful to compare ALS canopy height to the total basal area in forest plots. Fig. 7(b) shows the overall basal area for the five forest plots against average canopy height extracted from all ALS pixels within the plots. Because this takes into account areas of no trees, the basal area fractions are much lower than in Fig. 7(a), but the five datapoints fit a similar exponential trend.

4.3. Tree basal area vs. hemiphotos

The 2011 hemiphotos and manual tree measurements provide an opportunity to investigate how the hemispherical sky view from a site is related to the surrounding biomass. To do this, the *TBA* around a hemiphoto site (expressed as a fraction of ground area) was sampled by summing the *TBA* of all trunks within a certain radius of hemiphoto positions (Fig. 8(a)). Only the central four hemiphotos from each 2011 study plot (20 hemiphotos in all) were used because their positions allowed larger search radii (up to 6 m) to be tested while remaining within the 20 m × 20 m plot where *TBA* was measured (see Fig. 2(a)). Fig. 8(b) shows that the correlation

between v s and *TBA* becomes stronger (more negative) with increasing search radii, with a minimum at 5 m. Fig. 8(c) shows the strong linear relationship (r = −0.91) between v s and *TBA*for the 5 m search. These findings imply that sky view, which is crucial for radiative transfer, is affected by trees up to at least 5 m distance for this study area (this is likely to be different elsewhere depending on tree height). The flattening of the curve in Fig. 8(b) suggests that the effects of further away trees – which will be increasingly confined to the low horizon – is small.

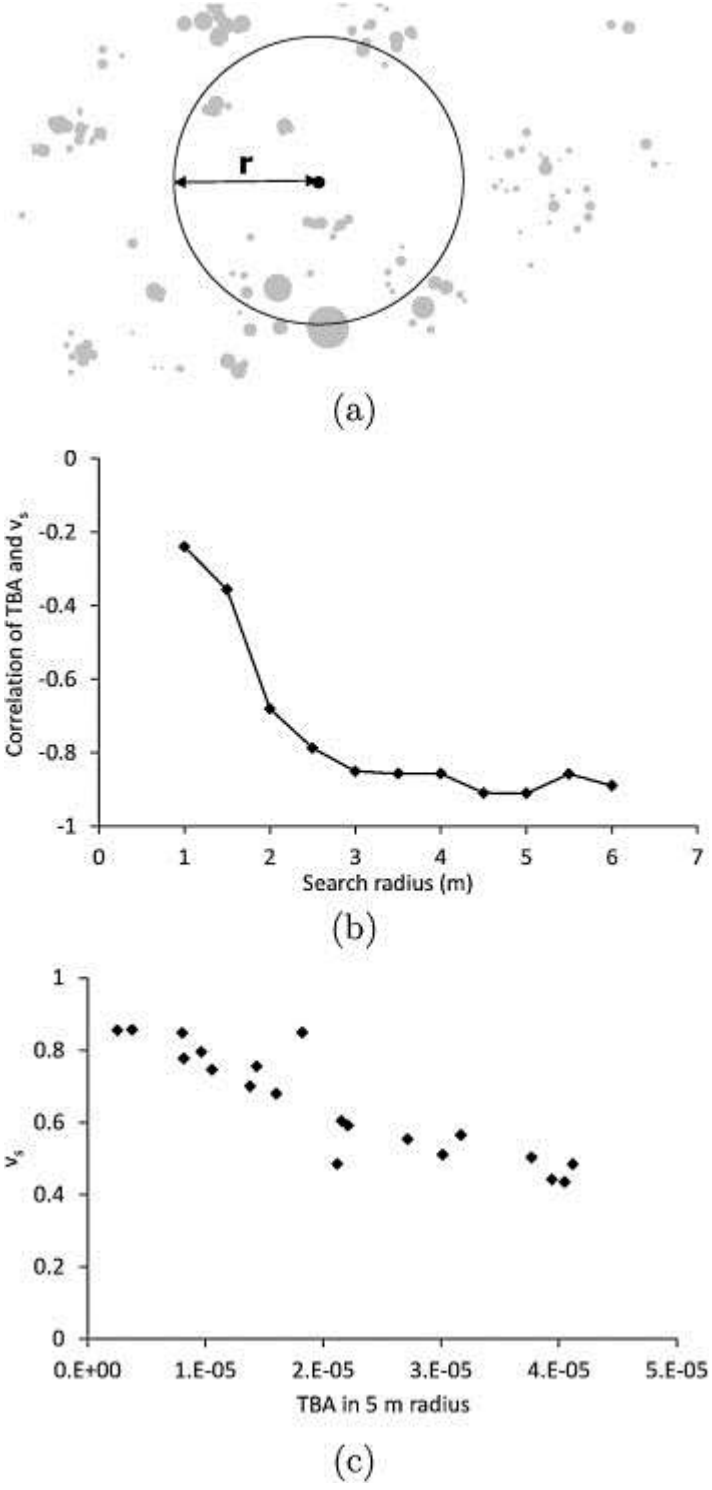

Fig. 8. (a) Schematic to show sampling of *TBA* in radius r from a hemiphoto site (trunk radii scaled up by factor of 5), (b) *TBA* /v s correlations for various search radii, and (c) v s vs. *TBA* for a 5 m search radius.

4.4. Hemiphotos vs. canopy height

For each of the 38 hemiphoto sites (5 from 2011 and 33 from 2012), the average values of v_s were calculated. For the same 38 sites, the ALS data were interrogated to extract the mean value of all canopy height datapoints within a chosen radius of the central hemiphoto site (co-ordinates 0, 0 in Fig. 2), following a method similar to Riaño et al. (2004). The effects of the chosen radius on the correlation of v_s with the extracted ALS canopy height are shown in Fig. 9(a). All the tested sample radii (3–30 m) produced significant correlations ($p < 0.01$). The best correlation was seen with a sample radius of 14 m, and this radius was used to extract values of average canopy height h for all the following calculations.

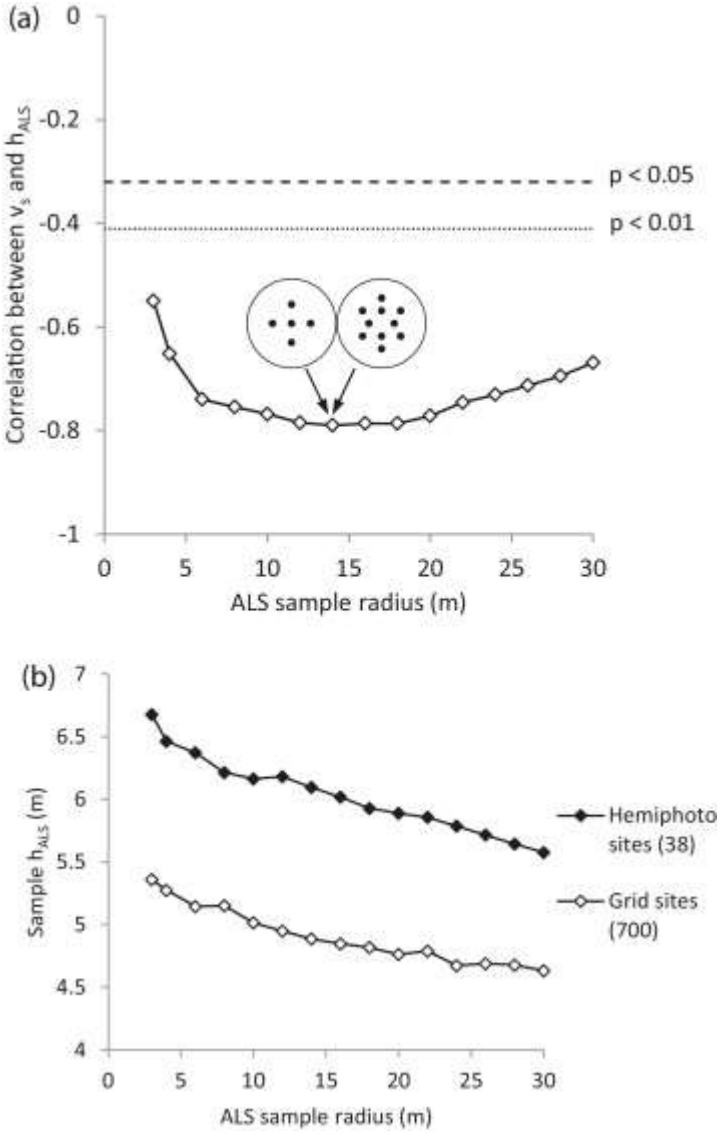

Fig. 9. (a) Correlation (r) with ALS canopy height for hemiphoto-derived v_s, for various ALS sample radii around the central hemiphoto points. Lines according to p-values of 0.05 and 0.01 are included. The inset scale drawings illustrate the best-correlating 14 m circle used to sample the plot-scale canopy height, and how it looks relative to the hemiphoto positions in Fig. 2 and (b) average sampled canopy height for the different sample radii, for the 38 hemiphoto sites and for 700 sites on a 2.5 km × 2.8 km grid with 100 m spacing (sampled canopy heights lower than 2 or greater than 15 m were not included).

As Fig. 9(b) shows, the average sampled canopy height across all 38 hemiphoto sites decreased with increasing sample radius. This is likely due to the heterogeneous nature of the forest cover; most sites were located within forest patches, and using wider radii sampled more pixels outside or nearer the edges of the forest patches where canopy height is lower, or zero. To assess whether this was representative of the wider area, 700 other points were sampled on a 2.5 km × 2.8 km grid with 100 m spacing extending to the furthest north, south, east and west extents of the hemiphoto sites (treeless sites were omitted by removing any points with canopy lower than 2 m). The average of these points showed a similar decreasing trend with increasing ALS sample radius, but the canopy height was generally lower by around 1 m; this difference is likely due to a bias for selecting hemiphoto sites closer to the centres of forest patches where trees were taller.

The correlations between ALS canopy height and vs in Fig. 9(a) prompt the development of simple models in order to predict the latter from the former over wider areas. Fig. 10 illustrates a simple approach in which the canopy is modelled as a homogeneous block of uniform thickness; the view at elevation angle θ has gap fraction $v\theta$ determined by:

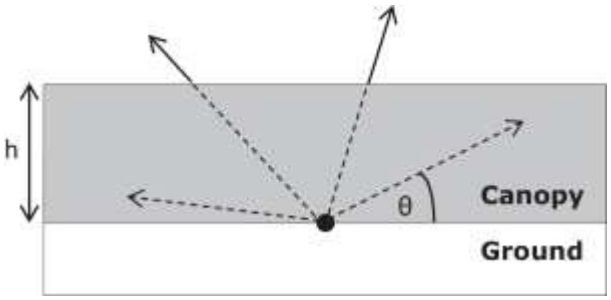

Fig. 10. Schematic of a 'homogeneous canopy' model.

$$v\theta = e^{-((\mu h)/(\sin\theta))}$$

where $h/(\sin\theta)$ is the pathlength through the canopy and μ is a bulk canopy extinction coefficient (m^{-1}). The corresponding vs can be calculated via an elliptic integral (Nijssen and Lettenmaier, 1999). Lawler and Link (2011) derived a value of $\mu = 0.2\ m^{-1}$ for dense conifer forest, while Link and Marks (1999) report values as low as $\mu = 0.03\ m^{-1}$ for low density conifers. Treating μ as a constant is suitable for homogeneous forest cover, but may be an over-simplification for patchy forest cover such as Abisko, where lower values of canopy height sampled from the ALS grid may actually represent areas where there are only a few scattered trees in the vicinity, and the low canopy height results from including tree-free pixels in the average. Such areas will likely have much higher overall gap fraction than the homogeneous approach of Fig. 10 would provide. To address this issue we propose that μ can be expressed as a function of two parameters:

equation(5)

$$\mu = \begin{cases} \dfrac{\mu_T}{h_T} h & \text{if } h < h_T \\ \mu_T & \text{otherwise} \end{cases}$$

such that μ increases linearly with canopy height up to a threshold height h_T, after which μ takes a constant value, μ_T. To test this concept, the following two models are examined:

• Model 1 – Eq. (4) taking μ as constant.
•Model 2 – Eq. (4) taking μ defined by Eq. (5).

where the names reflect the number of adjustable parameters in each model. Both models were fitted to the hemiphoto-derived v_θ for bands of 10° thickness. For Model 1, the optimal value of μ was 0.025 m^{-1}, while for Model 2 the optimal parameter values were μ_T = 0.029 m^{-1} and h_T = 6.8 m. Scatterplots of the 10° v_θ and overall v_s are shown in Fig. 11. Model 1 provides a decent fit to the hemiphoto gap fractions, but the v_s values follow a shallower slope than the 1:1 line; in particular v_s is somewhat underestimated for high gap fractions (low canopy) due to the arguments made above. By accounting for the sparse-canopy effects, Model 2 improves the fit as reflected in lower root mean square error RMSE from 0.056 to 0.049, and increased correlation coefficient from r = 0.81 to r = 0.83.

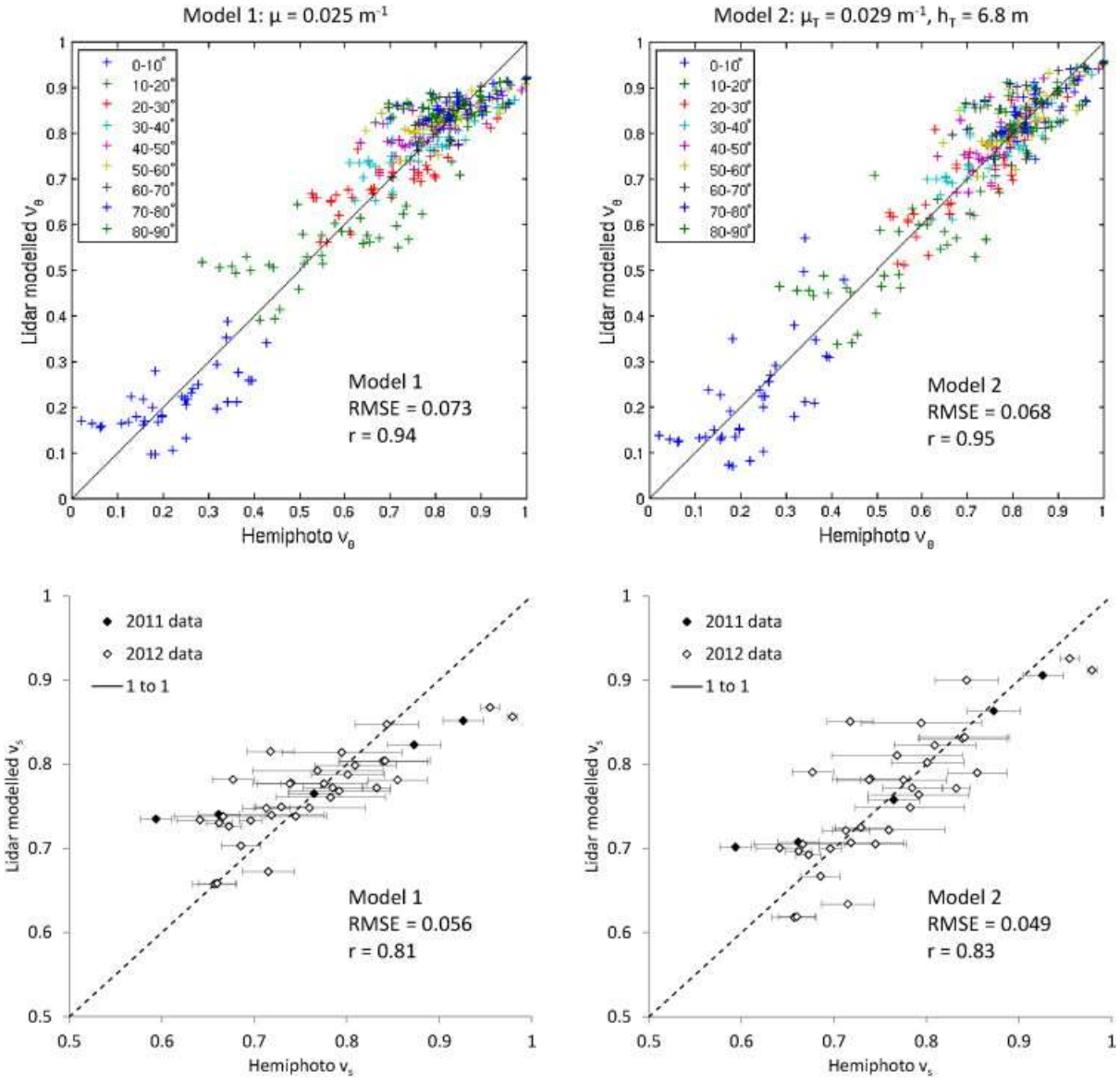

Fig. 11. Comparison of ALS-derived and hemiphoto-derived v_θ in 10-degree elevation bands (top) and v_s (bottom) for Model 1 and Model 2. Error bars represent standard error across all hemiphotos at each site (10 in 2011, 5 in 2012).

Fig. 12 shows the ALS canopy height for a 5 km × 3 km surveyed area, and the corresponding map of v_s calculated using Model 2. It is noted that this model does not take into account the effects of underlying topography; such effects were minimal for the hemiphoto sites which were all on quite flat terrain (maximum slope from the DEM of 8°), and as can be seen in Fig. 11 the models did not generally overestimate gap fraction at low elevation angles. In the context of wider distributed models, topography could be accounted for using larger-scale DEMs that would take into account mountains on the horizon to reduce incoming radiation before the application of the v_s map developed here. It should also be noted that towards and beyond the north-westernmost corner of the area in Fig. 12 some scattered coniferous trees (*Pinus sylvestris*) are present; the models developed here will likely not be appropriate for canopies of which these are a component.

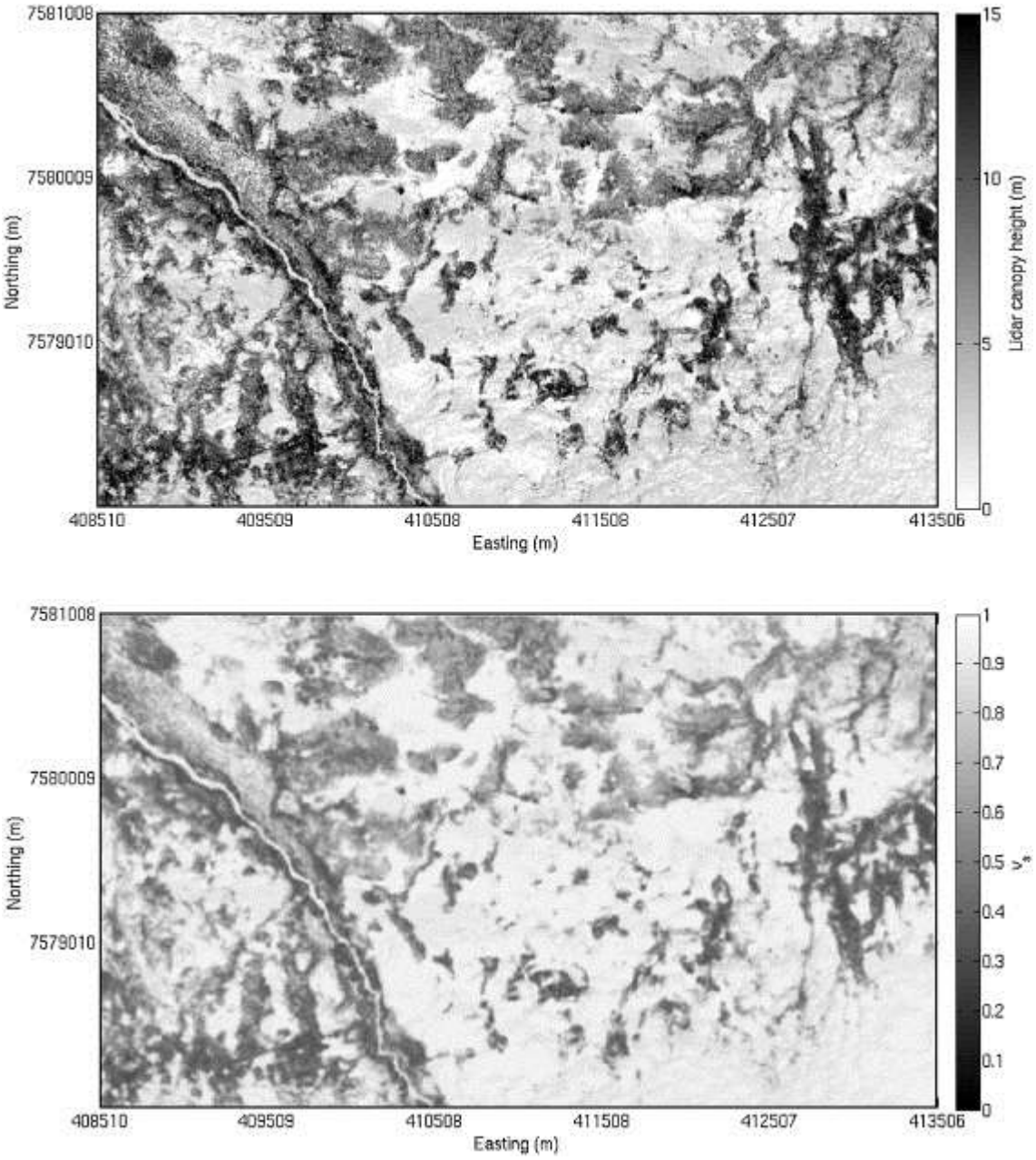

Fig. 12. ALS canopy height (top) and v s calculated using Model 2 (bottom) for the study area.

5. Discussion and conclusions

Extensive sets of ground measurements of leafless birch forest canopy have been compared to one another and to an ALS dataset for an area near Abisko, Sweden. Accurate canopy height derived from terrestrial laser scanning was shown to be useful for calibrating a map of ALS-derived canopy height. These canopy heights also exhibited strong spatial correlations with manually measured tree basal area, similar to those observed in previous large biometric surveys (Dahlberg et al., 2004). Basal area measurements showed strong correlations with hemiphoto-derived sky view fraction, and indicated that the sky view from a point on the snow surface was mainly influenced by trees within an immediate 5 m radius.

A simple slab-canopy model was developed to predict hemispherical sky view from ALS-derived canopy height. After some modifications to account for areas of sparse forest cover, the model was shown to match ground data accurately (RMSE < 5%), and used to produce 4 m raster grids of canopy sky view. If similar relationships could be obtained for other species, future efforts could combine such models with maps of land cover type for wide-scale quantification of radiative transfer to snow (Reid et al., 2013). The observed relationships between canopy height, hemispherical sky view and tree basal area imply that ALS could also be employed to estimate winter biomass across the region.

The general approach of sampling lidar-derived canopy heights around hemiphoto samples sites, with the lidar sampling radius adjusted to provide the best correlation, has been successfully applied in several studies on leafed forests, including Riaño et al. (2004), Morsdorf et al. (2006) and Richardson et al. (2009). The present study is, to the best of our knowledge, the first to show that a similar approach can be can be used to estimate the structural properties of a leafless winter canopy over wide scales.

Although such work is based on empirical relationships rather than detailed canopy structural models, the correlations are strong. The methods could provide a means of using low-resolution ALS data, similar to those becoming available for entire countries such as Finland, to upscale the results of ground surveys and smaller-scale high-resolution lidar surveys that provide greater canopy structural detail (Varhola et al., 2012 and Musselman et al., 2013).

Finally, this work shows that ALS data derived in summer can be used to extract bulk properties of the leafless winter canopy. Indeed, the summer foliage likely made the canopy height data more accurate; winter surveys of such sparse, twiggy trees would require far denser ALS sampling.

Acknowledgements

The research leading to these results received funding from INTERACT (Grant agreement no 262693), under the European Community's Seventh Framework Programme, as well as the UK's Natural Environment Research Council (NERC) Grant numbers NE/H008187/1 and NER/A/S/2001/00460. The authors would like to thank all the support staff at Abisko Scientific Research Station (ANS), as well as Maya King, Cécile Ménard, Mark Richardson and Melody Sandells for assistance in the field. Special thanks go to Ana Prieto-Blanco for initial processing of the ALS data. Aerial photography in Fig. 1 was collected as part of the NERC funded Arctic Biosphere-Atmosphere Coupling at mUltiple Scales (ABACUS) project by the University of Edinburgh's Diamond HK36 TTC-ECO aircraft; we thank John Moncrieff, Tom Wade, Mat Williams and Tim Hill for access to the imagery.

J. Bohlin, J. Wallerman, J.E.S. Fransson. Forest variable estimation using photogrammetric matching of digital aerial images in combination with a high-resolution dem. Scandinavian Journal of Forest Research, 27 (7) (2012), pp. 692–699

V. Brovkin, T. Raddatz, C.H. Reick, M. Claussen, V. Gayler. Global biogeophysical interactions between forest and climate. Geophysical Research Letters, 36 (2009), p. L07405

T.V. Callaghan, F. Bergholm, T.R. Christensen, C. Jonasson, U. Kokfelt, M. Johansson. A new climate era in the sub-arctic: accelerating climate changes and multiple impacts. Geophysical Research Letters, 37 (2010), p. L14705

J.-F. Cote, J.-L. Widlowski, R.A. Fournier, M.M. Verstraete

The structural and radiative consistency of three-dimensional tree reconstructions from terrestrial lidar. Remote Sensing of Environment, 113 (5) (2009), pp. 1067–1081.
U. Dahlberg, T. Berge, H. Petersson, C. Vencatasawmy. Modelling biomass and leaf area index in a sub-arctic scandinavian mountain area. Scandinavian Journal of Forest Research, 19 (1) (2004), pp. 60–71.

J.B. Drake, R.O. Dubayah, D.B. Clark, R.G. Knox, J. Blair, M.A. Hofton, R.L. Chazdon, J.F. Weishampel, S. Prince. Estimation of tropical forest structural characteristics using large-footprint lidar Remote Sensing of Environment, 79 (23) (2002), pp. 305–319.

R. Essery, P. Bunting, J. Hardy, T. Link, D. Marks, R. Melloh, J. Pomeroy, A. Rowlands, N. Rutter. Radiative transfer modeling of a coniferous canopy characterized by airborne remote sensing. Journal of Hydrometeorology, 9 (2) (2007), pp. 228–241.

R. Essery, J. Pomeroy, C. Ellis, T. Link. Modelling longwave radiation to snow beneath forest canopies using hemispherical photography or linear regression. Hydrological Processes, 22 (15) (2008), pp. 2788–2800.

S. Hancock, M. Disney, J.-P. Muller, P. Lewis, M. Foster. A threshold insensitive method for locating the forest canopy top with waveform lidar. Remote Sensing of Environment, 115 (2011), pp. 3286–3297.

S. Hancock, P. Lewis, M. Foster, M. Disney, J.-P. Muller. Measuring forests with dual wavelength lidar: a simulation study over topography. Agricultural and Forest Meteorology, 161 (2012), pp. 123–133.

J. Hardy, R. Melloh, G. Koenig, D. Marks, A. Winstral, J. Pomeroy, T. Link. Solar radiation transmission through conifer canopies. Agricultural and Forest Meteorology, 126 (3/4) (2004), pp. 257–270.

M. Hofton, J. Minster, J. Blair. Decomposition of laser altimeter waveforms. IEEE Transactions on Geoscience and Remote Sensing, 38 (4) (2000), pp. 1989–1996.

M. Hofton, L. Rocchio, J. Blair, R. Dubayah. Validation of vegetation canopy lidar sub-canopy topography measurements for a dense tropical forest. Journal of Geodynamics, 34 (34) (2002), pp. 491–502.

V. Kankare, M. Vastaranta, M. Holopainen, M. Räty, X. Yu, J. Hyyppä, H. Hyyppä, P. Alho, R. Viitala. Retrieval of forest aboveground biomass and stem volume with airborne scanning lidar Remote Sensing, 5 (5) (2013), pp. 2257–2274.

N. Kuusinen, P. Kolari, J. Levula, A. Porcar-Castell, P. Stenberg, F. Berninger. Seasonal variation in boreal pine forest albedo and effects of canopy snow on forest reflectance. Agricultural and Forest Meteorology, 164 (2012), pp. 53–60.

R.R. Lawler, T.E. Link. Quantification of incoming all-wave radiation in discontinuous forest canopies with application to snowmelt prediction. Hydrological Processes, 25 (21) (2011), pp. 3322–3331.

M.A. Lefsky, D. Harding, W. Cohen, G. Parker, H. Shugart. Surface lidar remote sensing of basal area and biomass in deciduous forests of eastern Maryland, USA. Remote Sensing of Environment, 67 (1) (1999), pp. 83–98.

Leica. Leica Cyclone 3D Point Cloud Processing Software (2013) http://hds.leica-geosystems.com/en/Leica-Cyclone_6515.htm

T. Link, D. Marks, J. Hardy. A deterministic method to characterize canopy radiative transfer properties. Hydrological Processes, 18 (18, SI) (2004), pp. 3583–3594.

T.E. Link, D. Marks. Point simulation of seasonal snow cover dynamics beneath boreal forest canopies. Journal of Geophysical Research: Atmospheres, 104 (D22) (1999), pp. 27841–27857.

V. Mahat, D.G. Tarboton. Canopy radiation transmission for an energy balance snowmelt model. Water Resources Research, 48 (2012) paper number W01534.

F. Morsdorf, B. Ktz, E. Meier, K. Itten, B. Allgwer. Estimation of LAI and fractional cover from small footprint airborne laser scanning data based on gap fraction. Remote Sensing of Environment, 104 (1) (2006), pp. 50–61.

K.N. Musselman, S.A. Margulis, N.P. Molotch. Estimation of solar direct beam transmittance of conifer canopies from airborne lidar. Remote Sensing of Environment, 136 (2013), pp. 402–415.

K.N. Musselman, N.P. Molotch, S.A. Margulis, P.B. Kirchner, R.C. Bales. Influence of canopy structure and direct beam solar irradiance on snowmelt rates in a mixed conifer forest. Agricultural and Forest Meteorology, 161 (2012), pp. 46–56.

K.N. Musselman, N.P. Molotch, S.A. Margulis, M. Lehning, D. Gustafsson. Improved snowmelt simulations with a canopy model forced with photo-derived direct beam canopy transmissivity Water Resources Research, 48 (2012), p. W10509.

E. Næsset, O.M. Bollandsås, T. Gobakken, T.G. Gregoire, G. Stahl. Model-assisted estimation of change in forest biomass over an 11 year period in a sample survey supported by airborne lidar: a case study with post-stratification to provide activity data. Remote Sensing of Environment, 128 (2013), pp. 299–314.

B. Nijssen, D.P. Lettenmaier. A simplified approach for predicting shortwave radiation transfer through boreal forest canopies. Journal of Geophysical Research, 104 (D22) (1999), pp. 27859–27868.

M. Nobis, U. Hunziker. Automatic thresholding for hemispherical canopy-photographs based on edge detection. Agricultural and Forest Meteorology, 128 (3/4) (2005), pp. 243–250.

M. Nyström, J. Holmgren, H. Olsson. Prediction of tree biomass in the forest tundra ecotone using airborne laser scanning. Remote Sensing of Environment, 123 (2012), pp. 271–279.

B. Pinty, J.-L. Widlowski, M.M. Verstraete, I. Andredakis, O. Arino, M. Clerici, T. Kaminski, M. Taberner. Snowy backgrounds enhance the absorption of visible light in forest canopies. Geophysical Research Letters, 38 (2011), p. L06404.

J.W. Pomeroy, D. Marks, T. Link, C. Ellis, J. Hardy, A. Rowlands, R. Granger. The impact of coniferous forest temperature on incoming longwave radiation to melting snow. Hydrological Processes, 23 (17) (2009), pp. 2513–2525.

W.H. Press, S.A. Teukolsky, W.T. Vetterling, B.P. Flannery. Numerical Recipes in C: The Art of Scientific Computing. (second ed.) Cambridge University Press, Cambridge, UK (1992).

W.G. Rees. Characterisation of arctic treelines by lidar and multispectral imagery. Polar Record, 43 (2007), pp. 345–352 10.

T. Reid, R. Essery. New methods to quantify canopy structure of leafless boreal birch forest from hemispherical photographs. Open Journal of Forestry, 3 (2) (2013), pp. 70–74.

T. Reid, R. Essery, N. Rutter, M. King. Data-driven modelling of shortwave radiation transfer to snow through boreal birch and conifer canopies. Hydrological Processes (2013) http://dx.doi.org.ezphost.dur.ac.uk/10.1002/hyp.9849 (in press).

D. Riaño, F. Valladares, S. Condés, E. Chuvieco. Estimation of leaf area index and covered ground from airborne laser scanner (lidar) in two contrasting forests. Agricultural and Forest Meteorology, 124 (34) (2004), pp. 269–275.

J.J. Richardson, L.M. Moskal, S.-H. Kim. Modeling approaches to estimate effective leaf area index from aerial discrete-return LIDAR. Agricultural and Forest Meteorology, 149 (67) (2009), pp. 1152–1160.

J.A.B. Rosette, P.R.J. North, J.C. Suárez. Vegetation height estimates for a mixed temperate forest using satellite laser altimetry. International Journal of Remote Sensing, 29 (5) (2008), pp. 1475–1493.

N. Rutter, R. Essery, J. Pomeroy, N. Altimir, K. Andreadis, I. Baker, A. Barr, P. Bartlett, A. Boone, H. Deng, H. Douville, E. Dutra, K. Elder, C. Ellis, X. Feng, A. Gelfan, A. Goodbody, Y. Gusev, D. Gustafsson, R. Hellstroem, Y. Hirabayashi, T. Hirota, T. Jonas, V. Koren, A. Kuragina, D. Lettenmaier, W.-P. Li, C. Luce, E. Martin, O. Nasonova, J. Pumpanen, R.D. Pyles, P. Samuelsson, M. Sandells, G. Schaedler, A. Shmakin, T.G. Smirnova, M. Staehli, R. Stoeckli, U. Strasser, H. Su, K. Suzuki, K. Takata, K. Tanaka, E. Thompson, T. Vesala, P. Viterbo, A. Wiltshire, K. Xia, Y. Xue, T. Yamazaki. Evaluation of forest snow processes models (SnowMIP2). Journal of Geophysical Research: Atmospheres, 114 (2009), p. D06111.

D. Seidel, S. Fleck, C. Leuschner. Analyzing forest canopies with ground-based laser scanning: a comparison with hemispherical photography. Agricultural and Forest Meteorology, 154–155 (2012), pp. 1–8.

J. Stoker, D. Harding, J. Parrish. The need for a national lidar dataset. Photogrammetric Engineering and Remote Sensing, 74 (9) (2008), pp. 1066–1068.

Swiss Federal Office of Topography. (2013) http://www.swisstopo.admin.ch

N. Thieme, O. Martin Bollandsas, T. Gobakken, E. Naesset. Detection of small single trees in the forest tundra ecotone using height values from airborne laser scanning. Canadian Journal of Remote Sensing, 37 (3) (2011), pp. 264–274.

A. Varhola, G.W. Frazer, P. Teti, N.C. Coops. Estimation of forest structure metrics relevant to hydrologic modelling using coordinate transformation of airborne laser scanning data. Hydrology and Earth System Sciences, 16 (10) (2012), pp. 3749–3766.

M. Vastaranta, M. Holopainen, M. Karjalainen, V. Kankare, J. Hyyppa, S. Kaasalainen. TerraSAR-X stereo radargrammetry and airborne scanning lidar height metrics in imputation of forest aboveground biomass and stem volume. IEEE Transactions on Geoscience and Remote Sensing, 52 (2013), pp. 1197–1204.

D.A. Zimble, D.L. Evans, G.C. Carlson, R.C. Parker, S.C. Grado, P.D. Gerard. Characterizing vertical forest structure using small-footprint airborne lidar. Remote Sensing of Environment, 87 (23) (2003), pp. 171–182.